The SKA-VLBI Perspective on Radio-Quiet AGNT

F. Panessa [1,†] T. An [2,3†] J. Petley [4,†] A. Wang [5,†] R. D. Baldi [6] E. Behar [7] E. K. Bempong-Manful [8,9] G. Bruni [1] N. Chang [10] S. Chen [7] L. Cui [10] F. D'Ammando [6] M. Kunert-Bajraszewska [11] S. Laha [12,13,14] A. Laor [7] M. Pérez-Torres [15,16] I. Prandoni [6] C. Ricci [17,18] and D. R. A. Williams-Baldwin [19]

[1] *INAF - Istituto di Astrofisica e Planetologia Spaziali, via del Fosso del Cavaliere 100, Roma, I-00133, Italy*
[2] *Department of Astronomy, University of Science and Technology of China, Hefei, Anhui 230026, China*
[3] *Shanghai Astronomical Observatory, Chinese Academy of Sciences, 80 Nandan Road, Shanghai 200030, China*
[4] *Leiden Observatory, Leiden University, Einsteinweg 55, 2333 CC Leiden, The Netherlands*
[5] *Key Laboratory of Particle Astrophysics, Institute of High Energy Physics, Chinese Academy of Sciences, Beijing 100049, China*
[6] *INAF - Istituto di Radioastronomia, via P. Gobetti 101, Bologna, I-40129, Italy*
[7] *Physics Department, Technion, Haifa, Israel*
[8] *Jodrell Bank Centre for Astrophysics, Alan Turing Building, School of Physics and Astronomy, University of Manchester, Manchester M13 9PL, UK*
[9] *School of Physics, University of Bristol, Tyndall Avenue, Bristol BS8 1TL, UK*
[10] *Xinjiang Astronomical Observatory, CAS, 150 Science-1 Street, Urumqi 830011, China*
[11] *Institute of Astronomy, Faculty of Physics, Astronomy and Informatics, NCU, Grudziądzka 5/7, 87-100, Toruń, Poland*
[12] *Astrophysics Science Division, NASA Goddard Space Flight Center, Greenbelt, MD 20771, USA.*
[13] *Center for Space Science and Technology, University of Maryland Baltimore County, 1000 Hilltop Circle, Baltimore, MD 21250, USA.*
[14] *Center for Research and Exploration in Space Science and Technology, NASA/GSFC, Greenbelt, Maryland 20771, USA*
[15] *Instituto de Astrofísica de Andalucía (IAA-CSIC), Glorieta de la Astronomía s/n, E-18008 Granada, Spain*
[16] *School of Sciences, European University Cyprus, Diogenes street, Engomi, 1516 Nicosia, Cyprus*
[17] *Department of Astronomy, University of Geneva, ch. d'Ecogia 16, 1290, Versoix, Switzerland*
[18] *Kavli Institute for Astronomy and Astrophysics, Peking University, Beijing 100871, China*
[19] *Jodrell Bank Centre for Astrophysics, School of Physics and Astronomy, The University of Manchester, Manchester, M13 9PL, UK*
[†] *Chapter co-ordinator*
E-mail: francesca.panessa@inaf.it, taoan3068@gmail.com, petley@strw.leidenuniv.nl, ailing.wang.wal@gmail.com, behar@physics.technion.ac.il, sina.chen@campus.technion.ac.il, laor@physics.technion.ac.il, emmanuel.bempong-manful@manchester.ac.uk, cuilang@xao.ac.cn, changning@xao.ac.cn

The accretion-ejection mechanism in Active Galactic Nuclei (AGN) remains a central open problem in astrophysics, tied to the role of AGN feedback in galaxy formation and evolution. Radio-quiet AGN dominate the observed AGN population. Lacking luminous jets, their radio emission traces a rich set of processes spanning the host galaxy kpc scales down to the vicinity of the supermassive black hole: star formation, AGN-driven winds and shocks, free-free emission from photo-ionized gas, low-power jets, and coronal activity close to the inner accretion disk. The Square Kilometre Array (SKA) will probe these processes across a wide frequency range with unprecedented sensitivity, wide-field survey capability, and, critically, high-resolution VLBI imaging. Flux, spectral, and polarization monitoring will constrain dynamics and environmental coupling, while mapping nuclear regions on sub-pc to kpc scales will disentangle compact cores from host emission, resolving the diversity of radio activity across accretion regimes and jet powers from the local Universe to the cosmic dawn. At the full AA4 deployment, the SKA-MID phased into global VLBI arrays will deliver sub-milliarcsecond imaging and μJy sensitivity over 0.35–15 GHz, enabling the first population-level census of radio-quiet AGN nuclei. Earlier AA* operations will support pilot studies of the brightest nearby systems.

1 Introduction

Active Galactic Nuclei (AGN) are among the most energetic long-lived sources in the Universe, powered by the accretion of matter onto Super Massive Black Holes (SMBHs) at the center of host galaxies. This accretion process releases vast amounts of energy across the entire electromagnetic spectrum, often profoundly shaping the evolution of the host galaxy through AGN feedback (e.g., Kormendy and Ho, 2013; Heckman and Best, 2014).

AGN have been historically classified based on the relative strength of their radio emission. The classic radio dichotomy was first formalized by Kellermann et al. (1989), who found a clear bimodal distribution in the ratio of radio to optical luminosity ($R \equiv f_{5\,\mathrm{GHz}}/f_B$). This divides the population into Radio-Loud (RL, $\sim$ 10%, $R \gtrsim 10$) and Radio-Quiet AGN (RQ, $\sim$ 90%, $R \lesssim 10$). RL AGN launch powerful, long-lived, highly collimated relativistic jets that frequently inflate kpc–Mpc radio lobes, show strong Doppler boosting, and can carry kinetic powers of $\sim 10^{44}$–10^{46} erg s^{-1} (Kellermann et al., 1989; Heckman and Best, 2014; Kormendy and Ho, 2013; Sikora et al., 2007; Blandford and Znajek, 1977). In contrast, RQ AGN typically host compact (sub-pc to kpc), lower-power outflows with mildly or intermittently relativistic motion (see Figure 1) (Wang et al., 2025, 2023b), weaker Doppler boosting (Sikora et al., 2007), lower brightness temperatures ($T_\mathrm{B} \lesssim 10^{7-9}$ K) (Nagar et al., 2002; Wang et al., 2023a,c; Chen et al., 2025), and little or no large-scale lobe development (Ulvestad and Wilson, 1984; Kellermann et al., 1989; Gallimore et al., 2004).

Although radio loudness is a convenient empirical metric, the spread across the AGN population more likely reflects variations in jet production efficiency, magnetic-flux supply, and accretion state, with Doppler boosting and host contamination further sculpting the observed distribution into an apparent bimodality (Sikora et al., 2007; Tchekhovskoy et al., 2011; Best and Heckman, 2012; Panessa et al., 2019; An, 2026). A complementary jetted/non-jetted classification has been advocated in which sources are separated by the presence of a resolved, high-brightness-temperature jet rather than by a luminosity ratio (Padovani et al., 2017a). A time-domain radio-loudness (TDRL) framework has recently been proposed to recast this dichotomy as an epoch-resolved, activity-state-dependent quantity, capturing sources whose apparent loudness migrates across the conventional boundary over an AGN duty cycle (An, 2026, in review). Throughout this chapter we retain the traditional $R < 10$ designation, noting that part of the RQ population is genuinely non-jetted, even at milliarcsecond angular resolution, while another part harbours jets that are confined, intermittent, or obscured.

Understanding the origin of the faint radio emission from RQ AGN is essential for a coherent picture of galaxy evolution. The RQ population makes up the vast majority of AGN, implying that their low-level radio emission is tied to the most common mode of SMBH accretion and feedback (e.g. Kharb and Silpa, 2023). The core challenge, therefore, lies in spatially, spectrally, and temporally resolving the weak signal that blends weak jets, disk–corona processes, winds, and circum-nuclear star formation into a single nuclear component (Panessa et al., 2019).

The most straightforward hypothesis is that RQ AGN still launch scaled-down relativistic jets. Lower jet power can result from limited magnetic-flux accumulation onto the black hole and from accretion states that increase mass loading or reduce magnetization, even if the spin plays

a non-negligible role (Blandford and Znajek, 1977; Narayan and Yi, 1995; Tchekhovskoy et al., 2011; McKinney et al., 2012; Sikora et al., 2007; Volonteri et al., 2007). Intermittent fueling and short duty cycles can also yield compact, transient ejections without sustained lobe inflation (**?**). In "frustrated" or "choked" scenarios, a dense, gas-rich circum-nuclear medium decelerates and disrupts the flow, with additional free–free absorption suppressing extended emission, so that the radio output remains confined to sub-parsec to parsec scales (Gallimore et al., 1996; O'Dea, 1998; Mukherjee et al., 2018; Wang et al., 2021). Such compact, persistent structures carry the signature of a self-absorbed synchrotron core with flat or inverted spectral index ($\alpha \gtrsim -0.5$, $F_\nu \sim \nu^\alpha$) (e.g., Baldi et al. 2022; Chen et al. 2025).

A second channel invokes powerful, non-relativistic outflows or winds launched from the accretion disk or the inner broad-line region. These high-velocity flows interact with the surrounding interstellar medium (ISM), generating shocks that accelerate relativistic electrons (e.g., Faucher-Giguère and Quataert 2012) and producing diffuse, steep-spectrum synchrotron radiation ($\alpha \approx -0.7$) potentially resolved on hundred-parsec scales, thereby serving as a direct tracer of large-scale AGN kinetic feedback (e.g., Harrison et al. 2018)

Another possible explanation for the observed radio signal is related to the intense star formation (SF) activity within the host galaxy (e.g., Padovani 2016). Radio emission from supernova remnants and HII regions is a well-established tracer of the Star Formation Rate (SFR), typically following a strong Far-Infrared (FIR)–radio correlation (e.g., Condon, 1992; Sargent et al., 2010). High angular resolution is necessary to disentangle this diffuse, galactic-scale emission from a point-like nuclear source (Kharb et al., 2006; Baldi et al., 2021; Cheng et al., 2025).

A physically distinct mechanism attributes the radio signal to the hot, magnetically dominated X-ray emitting corona located in the innermost regions close the black hole. This scenario suggests that magnetic reconnection events within the AGN corona can accelerate relativistic electrons, producing compact, highly variable, low-level radio emission (e.g., Laor and Behar, 2008). The emission may be gyro-synchrotron (non-thermal) radiation (e.g., Panessa et al., 2019), typically characterized by short-timescale flaring (Shablovinskaya et al., 2024), which distinguishes it from the steady-state emission of mini-jets or large-scale winds. Because it is anchored to the immediate SMBH environment, the coronal component offers a rare probe of the magnetic fields and energy dissipation close to the black hole event horizon. The millimeter-wave core emission, typically in the 100 – 300 GHz range, is tightly correlated with X-ray luminosity, supporting this scenario (Baldi et al., 2015; Petrucci et al., 2023; Ricci et al., 2023).

The prevalence of the RQ population is not constant across cosmic time. Observational evidence suggests that the comoving density of all AGN peaks at around redshift $z \sim 2$ (the cosmic noon), tracing the peak of star formation activity and black hole accretion (Croom et al., 2009; Aird et al., 2010; Madau and Dickinson, 2014). However, the precise evolutionary path and the physical processes driving the RQ fraction relative to the RL AGN, and their respective contributions of each to heating the circum-galactic medium, remain poorly constrained, particularly at high redshifts (Jiang et al., 2007; Kratzer and Richards, 2015; Keller et al., 2024). Since RQ AGN dominate the accreting black-hole budget over most of cosmic history, quantifying the origin of their radio emission is indispensable for assessing their true impact on galaxy evolution and the quenching of

star formation (Merloni and Heinz, 2008; Padovani et al., 2017b; Alexander et al., 2025; Prandoni et al., 2026).

The SKA, and especially its Very Large Baseline Interferometry (VLBI) mode, will deliver the sensitivity and resolution needed to break the present degeneracies between jet, wind, star-formation, and coronal origins of RQ radio emission. In this chapter, we outline the scientific capability of the SKA in this field, spanning a wide range of wavelengths and featuring strong performance, particularly as a VLBI element, the SKA will allow for a step change in our understanding of the origin and cosmic evolution of accretion and ejection in RQ AGN. The remainder of the chapter is organised as follows. Section 2 develops the accretion–ejection physics accessible to SKA–VLBI in the local Universe, with emphasis on brightness temperature, spectral, core shift and polarimetric discriminants that separate jet, corona, wind and star-formation origins. Section 3 extends the discussion to the early Universe, covering high-redshift quasars, the RQ AGN population identified in deep radio surveys, and the super-Eddington regime. Section 4 summarises the expected outcomes and the synergies with facilities operating in other wavebands.

At the AA4 stage, SKA-MID will operate with four VLBI-capable bands (1, 2, 5a, 5b) and provide tied-array beams feeding intercontinental baselines with the EVN and African partners; the Australian Long Baseline Array (LBA) provides the complementary southern-hemisphere coverage that is in fact geometrically better matched to the SKA–MID site, and we anticipate SKA–MID tied-array participation in LBA sessions to be a core mode of operation for RQ AGN at southern declinations. This configuration provides sub-milliarcsecond (sub-mas) resolution and μJy imaging sensitivity. The earlier AA* phase will allow focused observations of the brightest Seyferts and quasars, serving as a technical and scientific pathfinder for the full AA4 programme.

2 Accretion–ejection physics in the local Universe with SKA–VLBI capabilities

Prior to the advent of the SKA, interferometric observations of RQ AGN utilizing current facilities (e.g., VLA, e-MERLIN, GMRT, ATCA, EVN, VLBA, and LOFAR) have provided key constraints, yet have consistently highlighted the fundamental limitations in sensitivity and resolution needed to definitively disentangle emission sources (e.g., Panessa et al., 2019; Sebastian et al., 2020; Silpa et al., 2021b,a, 2022; Baldi et al., 2022; Kharb and Silpa, 2023; Chen et al., 2025).

VLBI studies of local Seyfert galaxies have established the ubiquity of compact sub-parsec cores with $T_{\rm B} \gtrsim 10^{6-7}$ K (Ulvestad et al., 1995; Ulvestad and Ho, 2001; Wang et al., 2023a,c; Cheng et al., 2025). In many cases, hints of parsec-scale jets or misaligned structures point to precession or jet–ISM interaction (Giroletti and Panessa, 2009; Panessa and Giroletti, 2013; Wang et al., 2021). In complete nearby samples, most VLA-detected nuclei are also detected with VLBI at 1.7 and/or 5 GHz, with typical core powers $\log P_{5\,\rm GHz} \sim 19.4\,\rm W\,Hz^{-1}$ and characteristic sizes of order 0.05 pc at 10 Mpc (Nagar et al., 2002, 2005; Panessa and Giroletti, 2013; Nyland et al., 2016; Cheng et al., 2025). These studies reveal a diversity of mechanisms, from jet-base synchrotron to steeper, shock-accelerated components. SKA–VLBI will systematically quantify their relative contributions across volume-limited samples rather than the handful of bright cases accessible today.

The nearby Universe provides the cleanest laboratory for disentangling the weak nuclear radio

emission of RQ AGN from circum-nuclear star formation and galactic-scale outflows. The critical missing capability has been the simultaneous provision of milli-arcsecond (mas) angular resolution to isolate the sub-parsec nucleus, μJy beam^{-1} sensitivity to detect compact components with brightness temperatures above the thermal regime, broad frequency coverage to separate synchrotron self-absorption from free–free and to perform Faraday diagnostics, and time-domain stability to track state changes in the accretion flow and flaring activity in the hot corona.

SKA–MID in its AA4 configuration, phased for integration into global VLBI networks, delivers exactly this combination: four initially deployed receiver bands (Bands 1, 2, 5a, 5b) spanning 0.35–15.4 GHz, connected-element baselines up to $\sim$ 150 km, and critically, tied-array beams that transform SKA-MID into an ultra-sensitive VLBI element on intercontinental baselines, delivering $\sim$ 1 mas at 8 GHz and better than 0.5 mas in Band 5b (8.3 – 15.4 GHz), providing linear scales of $\sim$ 0.1–1 pc at the typical distances of nearby galaxies ($z \lesssim 0.1$).

At these resolutions and sensitivities, the brightness temperature ($T_{\rm B}$) becomes the primary physical discriminant. Adopting a circular Gaussian source profile, a 30 μJy core at 10 GHz observed with a 0.5 mas beam yields $T_{\rm B} \approx 1.5 \times 10^6$ K, safely above H II / free–free values and in the regime of compact synchrotron emission; even a 20 μJy component at 5 GHz with a 1 mas beam yields $T_{\rm B} \approx 10^6$ K. With SKA–VLBI routinely reaching rms $\lesssim 1$ μJy beam^{-1} in 8 hrs, 5σ detections of 5–10 μJy cores are feasible, enabling the transition from mJy-biased pilot studies to a genuine census of nuclear radio components in intrinsically RQ systems.

2.1 SKA–VLBI capabilities to disentangle different radio emission mechanisms

Beyond detection, broadband imaging with the SKA Band 5 (4.6 – 15.4 GHz) coupled to Band 2 ($\simeq$1.3 – 1.7 GHz) provides spectral, opacity, and Faraday diagnostics central to classification (see Table 1). Exploiting the full scientific potential of this broadband capability demands that the partner VLBI stations (EVN, VLBA, African VLBI Network, LBA) deliver contemporaneous coverage matched to the SKA–MID frequency range. This carries concrete programmatic implications for the upgrade path of the non-SKA elements, and we flag it here as a prerequisite for core-shift and Faraday tomography at the precision discussed below. Compact jet bases are expected to show flat or slightly inverted spectra at cm wavelengths due to synchrotron self-absorption, with frequency-dependent core positions $r_{\rm core}(\nu) \propto \nu^{-1/k}$, encoding particle density and magnetic-field gradients near the launch region (Lobanov, 1998). Measurement of core shifts between 8 and 15 GHz at the level of tens of μas is realistic with phase-referenced SKA–VLBI, allowing direct estimates of the magnetic field (B) and pressure near $\sim 10^{3-4}\, R_{\rm g}$ (where $R_{\rm g} = GM_\bullet/c^2$ is the gravitational radius). The same wideband datasets, recorded in full Stokes, yield rotation-measure (RM) maps and polarization morphologies that distinguish ordered fields in a collimating jet from the patchier, more depolarizing patterns associated with wind shocks (Hovatta et al., 2012; Mahmud et al., 2013).

Time-domain capability will be transformative for identifying transient jet or coronal events. The well-established radio–X-ray correlation in RQ quasars, $L_{\rm R} \sim 10^{-5}\, L_{\rm X}$ (the AGN analogue of the Güdel–Benz relation), argues that at least part of the RQ nuclear emission arises in a magnetized disk corona (Laor and Behar, 2008; Behar et al., 2015, 2018; Panessa et al., 2019). Coordinated, high-cadence SKA–VLBI monitoring during X-ray bright phases can test whether radio-quiet

nuclei display the same disc–corona–jet coupling phenomenology seen in radio-loud objects and X-ray binaries: core brightening and spectral hardening during the rising phase, followed by the appearance of new mas-scale components and evolving polarization as energy is redistributed. Correlating SKA–VLBI variability and core-shift evolution with X-ray spectral state transitions will discriminate between corona-dominated emission and contributions from low-power jets or winds. In addition, high-cadence monitoring campaigns with sufficient sensitivity to detect rapid, low-level flaring from magnetic reconnection events in the accretion disk corona will open a largely unexplored time-domain window on RQ nuclear activity.

A critical confounding factor at arcsecond resolution is host-galaxy emission: diffuse synchrotron from star formation follows the FIR–radio correlation and can dominate the total 1–3 GHz flux (Condon, 1992). SKA–VLBI overcomes this by resolving out the kpc-scale disk and recovering the nuclear SED at mas scales; matched-*uv* connected-element imaging at sub-arcsecond resolution provides stringent host subtraction. Where the residual, resolved-out emission follows the FIR–radio relation, we attribute it to star formation; where it correlates with optical outflows, steep spectra, and edge-brightened kinematics, we identify AGN-driven wind shocks as the dominant extended component (Harrison et al., 2018; Wang et al., 2023c). In either case, nuclear compactness and $T_{\rm B}$ remain the definitive indicators of an AGN origin.

The wind-shock interpretation carries broader physical significance because energy-conserving outflows efficiently convert a fraction of the AGN luminosity into mechanical work, boosting momentum flux on kpc scales and producing steep-spectrum radio emission at outflow edges (Harrison et al., 2014; Morganti et al., 2015; Jarvis et al., 2019). Spatially resolved studies with VLA, MeerKAT, and e-MERLIN have revealed diffuse, polarized structures co-spatial with ionized or molecular outflow cones in several nearby Seyferts and quasars, showing rotation-measure (RM) and depolarization behavior distinct from collimated jet bases (Gallimore et al., 2006; Barcos-Muñoz et al., 2018; Mingo et al., 2022). The Quasar Feedback Survey has proven especially powerful in this regard, combining spatially resolved radio continuum, polarimetry, and optical integral-field data to isolate jet-, wind-, and star-formation-dominated components across a homogeneous sample of obscured $z \lesssim 0.2$ AGN (Jarvis et al., 2019; Silpa et al., 2022); the survey's rotation-measure results demonstrate that depolarization asymmetries and RM gradients can unambiguously separate collimated low-power jets from mass-loaded wind shocks in sources even when the total-intensity morphology alone remains degenerate (Sebastian et al., 2020; Silpa et al., 2021b,a; Kharb and Silpa, 2023). If such signatures proven common among local RQ AGN, winds must account for a significant fraction of their radio power budget.

At mas scales, SKA–VLBI resolution can resolve the base of wide-angle outflows on parsec scales, providing direct observational benchmarks for numerical simulations of line-driven or magnetic winds. This high resolution will help distinguish between a persistent jet and the initial expansion of a nuclear wind/shock region. Moreover, the SKA offers excellent polarimetric capabilities that can reveal the ordered magnetic fields near the SMBH, a governing factor in jet formation. Mas-scale polarization mapping of the compact cores will constrain the magnetic field topology responsible for launching the jet or wind.

The SKA's superior polarimetric capabilities (rms noise less than a few μJy beam^{-1} in full Stokes)

Table 1: SKA–VLBI diagnostics for radio-quiet AGN emission mechanisms.

Mechanism	Primary Physical Origin	Characteristic Observational Signatures (Pre-SKA)	Key SKA–VLBI Requirements & Estimates
Jets/Jet base	Scaled-down, mildly relativistic, collimated outflow from the accretion disk base.	**Morphology**: Compact core, unresolved, or core-jet structure ($<$ 1 pc). **Spectrum**: Core: Flat or inverted ($\alpha \gtrsim -0.5$), SSA emission. Jet: optically thin steep spectrum. **Kinematics**: Proper motion detected	**Resolution**: $\lesssim$ 1 mas imaging. **Sensitivity**: $\sim \mu$Jy (AA4) to detect faint cores. **Diagnostic**: Measure knot motions, map polarization structure
Corona	Non-thermal/thermal processes (magnetic reconnection) in the hot, compact accretion disk corona.	**Morphology**: Ultra-compact ($<$ 0.1 pc), unresolved core. **Spectrum**: Flat/inverted ($L_R/L_X \sim 10^{-5}$). **Kinematics**: Expected rapid, non-steady flaring/variability.	**Resolution**: Required $\lesssim$ 1 mas resolution to isolate the compact source. **Sensitivity**: High cadence monitoring; μJy detection for variability. **Diagnostic**: Simultaneous X-ray/radio monitoring to test the Neupert effect.
Winds	Synchrotron emission from shocks generated as an uncollimated AGN outflow interacts with the ISM.	**Morphology**: Diffuse, irregular structures, extending $\sim$ 100 pc. **Spectrum**: Steep ($\alpha \approx -0.7$), optically thin. **Kinematics**: Slow bulk speeds.	**Resolution**: High mas-resolution needed to resolve the outflow base from the jet region. **Sensitivity**: $\sim 2\,\mu\mathrm{Jy\,beam^{-1}}$ (SKA–Low) for faint relic/shocked plasma. **Diagnostic**: Polarization mapping (Faraday RM).
Star Formation	Diffuse synchrotron emission from supernova remnants and thermal free-free from HII regions.	**Morphology**: Diffuse, host-like (kpc scales). **Spectrum**: Steep ($\alpha \approx -0.7$), matching the FIR-radio correlation. **Kinematics**: Non-variable; highly depolarized.	**Resolution**: $\lesssim$ 1 mas resolution is necessary to resolve out the extended background. **Sensitivity**: $\sim \mu$Jy sensitivity ensures the faint nuclear component is cleanly isolated. **Diagnostic**: Spectral index mapping and spatial correlation with FIR tracers.

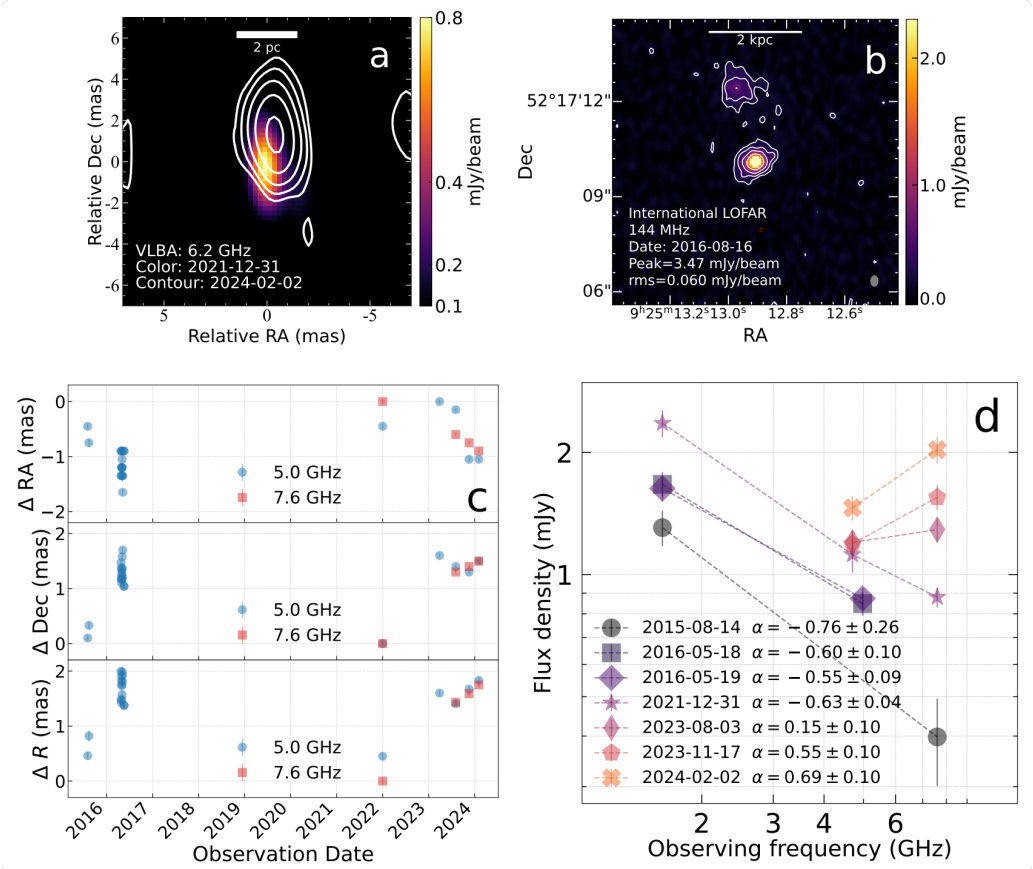

Figure 1: VLBI evidence that a subset of RQ AGN launches relativistic jets, illustrated by Mrk 110 as a representative case (taken from Wang et al. (2025)). (a) VLBA 6.2 GHz images on 2021 December 31 (colour scale) and 2024 February 2 (contours), revealing a core offset of $\sim$ 1.6 mas. The image centre is set at the 2021 December peak position (R.A. 09:25:12.84781, Dec. +52:17:10.3862). (b) International LOFAR image at 144 MHz observed on 2016 August 16, revealing a $\sim$ 1.7 kpc northern extension aligned with the parsec-scale jet. (c) Peak-position evolution. (d) Radio-spectrum evolution from 2015 to 2024, documenting a transformation from a steep ($\alpha = -0.76$) to an inverted ($\alpha = +0.69$) spectral index. Historical data from 2015–2016 are from Panessa et al. (2022); dashed lines are power-law fits. This source exemplifies the class of measurement (compactness, core shift, spectral inversion, and proper motion) that SKA–VLBI will deliver for volume-limited samples, extending such diagnostics well beyond the few bright cases currently accessible.

will allow enable detailed mapping of the strength and geometry of magnetic fields in the circum-nuclear medium. Synchrotron emission generated by wind-shock acceleration is expected to be co-spatial with known outflows (traced by multi-wavelength data) but exhibit a distinct polarization morphology and magnetic field structure compared to highly organized, relativistic jets (Alexander et al., 2025; Kudoh et al., 2026).

The contrast in radio polarization offers a key discriminant between physical mechanisms powering the sub-parsec core. Flat-spectrum, gr-T_B cores exhibiting that exhibit negligible or extremely low polarization levels constitute the expected accretion-disk corona model. This low polarization

results from the emission being generated in an isotropic or quasi-spherical region, leading to the cancellation of the total electric vector polarization across different viewing angles (Laor and Behar, 2008; Behar et al., 2015; Inoue and Doi, 2018; Baldi et al., 2021; Chen et al., 2023; Wang et al., 2023a,c).

Conversely, the observation of cores displaying detectable, ordered polarization (even if low) and systematic core shifts would favor a low power jet model. These features are characteristic of synchrotron self-absorbed jet bases, where the magnetic field structure is ordered, and the emission is produced in a collimated outflow (Panessa et al., 2019). Sebastian et al. (2020) and Silpa et al. (2021a) provide observational support for this discriminator by recovering ordered polarization structures and non-zero rotation measures in compact, flat-spectrum Seyfert cores where the coronal model would predict negligible polarization.

A single SKA–VLBI observation simultaneously delivers mas-scale morphology, a spectral index spanning Band 2 to Band 5a, and full-Stokes polarimetry; only when all three diagnostics are available in concert can the coronal and low-power-jet hypotheses for the compact nucleus of a radio-quiet AGN be reliably separated. The power of this approach rests not on the production of a single dataset *per se*, but on the fact that the three discriminants carry independent systematics and respond differently to source state, so that cross-comparison eliminates degeneracies that any individual diagnostic would leave unresolved.

Operationally, the SKA–VLBI strength lies in a stable, wideband, full-polarization calibration and the ability to phase SKA–MID into EVN and VLBA sessions, with the LBA providing the analogous function for southern targets. Modern, reproducible pipelines such as rPICARD and GPCAL have been validated on comparable broadband datasets and support absolute EVPA tying across bands (Janssen et al., 2019; Kim et al., 2024). With phase referencing to nearby calibrators and contemporaneous multi-frequency registration, positional shifts of order 10–50 μas can be recovered across 5–8 GHz where the partner VLBI arrays provide adequate baseline coverage, permitting magnetic-field and pressure gradients to be inferred near the jet base.

A natural observing program is a volume-limited ($D \lesssim 100$ Mpc) sample of nearby Seyferts and high-$L/L_{\rm Edd}$ RQ AGN observed with SKA–VLBI at Band 5 for the core/jet base and polarization, and Band 2 for opacity and RM, with 8–10 epochs over a year and μJy-level sensitivity per epoch. For typical 20–50 μJy cores at 5–10 GHz, we expect $T_{\rm B} \sim 10^6$ K at 1 mas and ~ 4 times higher at 0.5 mas, ensuring separation from thermal processes. Simultaneous X-ray monitoring tests whether radio/opacity changes track coronal state, while ALMA/mm monitoring probes the putative coronal synchrotron component that often peaks near 100 GHz (Baldi et al., 2015; Behar et al., 2015, 2018; Inoue and Doi, 2018; Petrucci et al., 2023; Shablovinskaya et al., 2024; Mutie et al., 2025; del Palacio et al., 2025). Detections of core shifts at the 30–100 μas level between 8 and 15 GHz, if accompanied by spectral flattening and ordered polarization during bright phases, would constitute evidence for magnetically dominated launch episodes. Strong depolarization with enhanced RM and stalled morphology would favor mass-loaded winds. Either outcome tightens the constraints on disc–jet (or disc–wind) coupling in the RQ regime.

Finally, SKA–VLBI enables a clean test of whether the RQ population adheres to the black-hole

fundamental plane that relates radio luminosity, X-rays, and mass (Merloni et al., 2003; Saikia et al., 2018; Ruffa et al., 2023).This relationship appears to hold down to stellar-mass black holes, but the scatter can be significantly reduced by assembling a large, well-defined and unbiased sample of radio detections of low-mass SMBHs associated with RQ AGN (Plotkin et al., 2012; Gültekin et al., 2022; Wang et al., 2024). By delivering nuclear-only radio measurements with known T_B and morphology, SKA–VLBI can either confirm that RQ nuclei obey the same accretion–ejection scalings as their radio-loud counterparts, or reveal a genuine bifurcation tied to magnetization and launch efficiency at low jet powers.

3 Radio activity in the early Universe

Understanding RQ AGN beyond $z \sim 3$ is key to tracing the evolution of low-power jets and magnetic flux across cosmic time. Since the angular diameter distance reaches a maximum around $z \approx 1.5$, the power of VLBI to study AGN accretion and ejection physics on sub-galaxy scales at high redshift is only limited by the luminosity of the sources available to us and the sensitivity of our telescopes. The AA4 array will allow observations with SKA–MID at a resolution ranging from $0.3''$ to $0.03''$, while for SKA-LOW the range is $10''$ to $2''$. When incorporated into a VLBI network, SKA-MID achieves image-plane resolutions of 1–10 μas as at rms sensitivities of a few μJy beam^{-1}(Li et al., 2024). The challenge for VLBI SKA-LOW is more significant, since fewer sites operate globally at these frequencies; however, with the potential to study intrinsically fainter sources, thanks to the synchrotron power law slope, it could still be crucial to the study of RQ AGN at high redshift (Kondapally et al., 2026; Spingola et al., 2026). SKA–LOW offers enormous survey speed but faces a confusion-limited floor at arcminute-to-arcsecond scales unless very long baselines are available; consequently, SKA–LOW will be superb for demographics and spectral curvature, while SKA–MID + VLBI provides the compactness, brightness temperature, polarization, and core-shift diagnostics needed to isolate the nucleus.

Separating radio emission from star formation and AGN activity will become an ever greater challenge with the SKA. Particularly for SKA-LOW, without an improvement in resolution, AGN studies will be severely limited by confusion noise, and it will be difficult to progress past LOFAR deep surveys apart from surveying more quickly and in the southern hemisphere.

3.1 Quasars

For luminous quasars at $z \gtrsim 6$, the most open issues are the prevalence and duty cycle of relativistic outflows at the lowest detectable powers, and the physical origin of the faint radio population that dominates deep counts. Current constraints on the radio-loud fraction at the highest redshifts remain limited by sensitivity and sample size (Bañados et al., 2015; Perger et al., 2017). Existing VLA surveys produce few detections at ~100–200 μJy and large uncertainties, while VLBI detections of individual sources confirm compact, high-T_B cores consistent with jet bases (An et al., 2020, 2023; Belladitta et al., 2023, 2020; Frey et al., 2011, 2024; Liu et al., 2022a,b, 2024; Ighina et al., 2021; Momjian et al., 2018; Sbarrato et al., 2012; Spingola et al., 2020; Radcliffe et al., 2021).

SKA refines the question from "*are jets present?*" to "*how do they couple to the flow and environment?*". Not going into details about sensitivity limits here, we emphasize the diagnostics that

uniquely matter at high z. Nuclear compactness and spectral shape on parsec scales reveal the nature of the central engine, while wide-band polarization and Faraday rotation measures trace magnetized screens threading the inner few hundred parsecs. Multi-frequency phase registration further recovers *core shifts* that encode opacity and B-field gradients along the jet, directly testing launching scenarios under the intense radiative and IC/CMB losses expected at these redshifts (Ghisellini et al., 2014; **?**; **?**). Paired LOW+MID connected-element imaging then ties the parsec-scale core to any steep, edge-brightened structures associated with quasar-driven winds, placing the faint radio output of the majority population on a firm physical footing.

Beyond direct source characterization, compact high-z quasars selected and characterized by SKA–VLBI provide the bright, stable backlights needed for HI 21-cm absorption experiments and tomography during reionization, while their RM and depolarization patterns probe the early magnetized CGM/IGM (Miley and De Breuck, 2008; Mesinger et al., 2016). In combination with JWST/ALMA constraints on host gas and star formation, SKA will establish whether the typical high-z quasar is best described by a weak, intermittently mass-loaded jet (or wind) anchored in a magnetized corona, or by truly jetless accretion whose radio output is dominated by wind shocks and circumnuclear star formation. This distinction is only accessible with the multi-scale, polarization-aware view that the SKA provides.

3.2 Radio-Quiet AGN

The prospect of studying RQ AGN is bolstered by the classification of sources in deep radio images taken by SKA pathfinders. For example, Best et al. (2023) classified $\sim 80,000$ sources in the first LoTSS: Deep Fields data release using several SED fitting codes to find star-forming galaxies, Low Exitation Radio Galaxies, High Exitation Radio Galaxies and RQ AGN. They found that the RQ AGN fraction grows from less than 10% at $z = 1$ to more than 30% by $z = 4$ while other populations decrease. Given that the multi-wavelength information needed to estimate star formation rates will become sparser at high-redshift, brightness temperature measurements using SKA–VLBI may become the only way to separate AGN and star formation radio emission for these distant radio-quiet sources.

Extrapolations from LoTSS-Deep and MIGHTEE luminosity functions indicate that, within a $100\,\mathrm{deg}^2$ SKA–LOW field reaching $5\,\mu\mathrm{Jy\,beam}^{-1}$, several $\times 10^4$ radio-quiet AGN will be detected up to $z \sim 4$ (Hale et al., 2025), with a few hundred compact enough for VLBI follow-up. Such statistics will, for the first time, enable population-level tests of jet duty cycles, magnetic-field evolution, and feedback efficiency across cosmic time (Hardcastle et al., 2026).

4 Conclusions and Future Synergies for RQ AGN Research

The field of RQ AGN is poised for a major transformation, moving beyond the current limitations imposed by low sensitivity and insufficient angular resolution. The fundamental ambiguity, whether the core radio emission originates from scaled-down relativistic jets, a hot magnetized accretion disk corona, or kinetic wind shocks, will be resolved by the SKA. SKA–VLBI is the key differentiator here, as it enables a statistically complete census of nuclear components. The SKA-Mid AA4 configuration will achieve ~ 1 mas imaging at 5 GHz with a thermal rms of a few $\mu\mathrm{Jy\,beam}^{-1}\,\mathrm{hr}^{-1}$

(deeper limits are reached only in long integrations), providing the resolution to measure knot motions and derive fundamental properties like the magnetic field and degree of polarization on parsec scales. This kinematic and spectral precision is essential for distinguishing true jet activity from coronal emission. Furthermore, the exquisite sensitivity of SKA-VLBI polarimetry will allow detailed studies of the magnetic-field structure, directly testing the coronal versus jet launch scenarios. The full power of the SKA is realized through multi-frequency synergies. Coordinated X-ray (e.g., NewAthena, Einstein Probe) and mm/sub-mm (ALMA, ngVLA) monitoring, combined with optical/IR IFU spectroscopy (JWST, MUSE) and optical/NIR light curves (LSST) will tie SKA-VLBI nuclear diagnostics to coronal heating, wind energetics, and host feedback. GRMHD and polarized radiative-transfer simulations will interpret SKA polarization and core-shift data in terms of magnetic flux and mass-loading at the jet base. By applying these multi-domain diagnostics, the SKA will enable the physical classification of the RQ AGN population, advancing the field from conjecture to a quantitative, multi-mechanism understanding of accretion and feedback physics in the dominant class of AGN.

Several plausible enhancements would extend the RQ AGN science case beyond what AA4 already delivers. A Band 6 receiver (or SKA–MID participation in mm VLBI through dedicated front-ends) would connect the self-absorbed cm cores measured here to the optically thin mm regime where the putative coronal synchrotron component peaks, bridging the frequency gap to ALMA at the scale of the jet launch region. Higher-time-resolution voltage-buffer recording would enable sub-second coronal flare studies coordinated with Einstein Probe and NewAthena triggers, probing variability at cadences shorter than the ∼few-minute integrations that set the thermal noise floor in standard VLBI. Extended baselines, in particular participation in mm space-VLBI missions or long-baseline additions in Africa, would push the angular resolution into the tens of μas regime required to resolve the jet base of a nearby Seyfert at 10^2–10^3 R_g (Bempong-Manful et al., 2026). Each of these capabilities is an incremental upgrade to the AA4 baseline rather than a replacement, and each targets a specific measurement whose cost–benefit can be evaluated against the first-generation AA4 results.

Acknowledgements

FP and GB acknowledge financial support from the Bando Ricerca Fondamentale INAF and "Programma di Ricerca Fondamentale INAF 2023 and 2024. E.B. is supported by The Israel Science Foundation (grant No. 2617/25).

References

J. Aird et al. *MNRAS*, 401(4):2531–2551, Feb. 2010. doi: 10.1111/j.1365-2966.2009.15829.x.

D. M. Alexander et al. *New Astron. Rev.*, 101:101733, Dec. 2025. doi: 10.1016/j.newar.2025.101733.

T. An. *ApJL*, 1004(1):L5, June 2026. doi: 10.3847/2041-8213/ae6cde.

T. An et al. *Nature Communications*, 11:143, Jan. 2020. doi: 10.1038/s41467-019-14093-2.

T. An et al. *MNRAS*, 519(3):4047–4055, Mar. 2023. doi: 10.1093/mnras/stac3774.

E. Bañados et al. *ApJ*, 804(2):118, May 2015. doi: 10.1088/0004-637X/804/2/118.

R. D. Baldi, E. Behar, A. Laor, and A. Horesh. *MNRAS*, 454(4):4277–4281, Dec. 2015. doi: 10.1093/mnras/stv2284.
R. D. Baldi et al. *MNRAS*, 508(2):2019–2038, Dec. 2021. doi: 10.1093/mnras/stab2613.
R. D. Baldi et al. *MNRAS*, 510(1):1043–1058, Feb. 2022. doi: 10.1093/mnras/stab3445.
L. Barcos-Muñoz et al. *ApJL*, 853(2):L28, Feb. 2018. doi: 10.3847/2041-8213/aaa28d.
E. Behar et al. *MNRAS*, 451(1):517–526, July 2015. doi: 10.1093/mnras/stv988.
E. Behar et al. *MNRAS*, 478(1):399–406, July 2018. doi: 10.1093/mnras/sty850.
S. Belladitta et al. *A&A*, 635:L7, Mar. 2020. doi: 10.1051/0004-6361/201937395.
S. Belladitta et al. *A&A*, 669:A134, Jan. 2023. doi: 10.1051/0004-6361/202243855.
E. Bempong-Manful et al. In *Advancing Astrophysics with the SKA – II (AASKAII)*. 2026. arXiv search: Report number AASKAII/Bempong-Manful01.
P. N. Best and T. M. Heckman. *MNRAS*, 421(2):1569–1582, Apr. 2012. doi: 10.1111/j.1365-2966.2012.20414.x.
P. N. Best et al. *MNRAS*, 523(2):1729–1755, 2023. ISSN 13652966. doi: 10.1093/mnras/stad1308. URL https://ui.adsabs.harvard.edu/abs/2023MNRAS.523.1729B/abstract. Publisher: Oxford University Press.
R. D. Blandford and R. L. Znajek. *MNRAS*, 179:433–456, May 1977. doi: 10.1093/mnras/179.3.433.
S. Chen et al. *MNRAS*, 525(1):164–182, Oct. 2023. doi: 10.1093/mnras/stad2289.
S. Chen et al. *ApJ*, 979(2):241, Feb. 2025. doi: 10.3847/1538-4357/ada142.
X. Cheng et al. *ApJSS*, 277(2):56, Apr. 2025. doi: 10.3847/1538-4365/adba4c.
J. J. Condon. *ARA&A*, 30:575–611, Jan. 1992. doi: 10.1146/annurev.aa.30.090192.003043.
S. M. Croom et al. *MNRAS*, 399(4):1755–1772, Nov. 2009. doi: 10.1111/j.1365-2966.2009.15398.x.
S. del Palacio et al. *A&A*, 701:A41, Sept. 2025. doi: 10.1051/0004-6361/202554936.
C.-A. Faucher-Giguère and E. Quataert. *MNRAS*, 425(1):605–622, Sept. 2012. doi: 10.1111/j.1365-2966.2012.21512.x.
S. Frey et al. *A&A*, 531:L5, July 2011. doi: 10.1051/0004-6361/201117341.
S. Frey et al. *A&A*, 681:L12, Jan. 2024. doi: 10.1051/0004-6361/202348602.
J. F. Gallimore, S. A. Baum, C. P. O'Dea, and A. Pedlar. *ApJ*, 458:136, Feb. 1996. doi: 10.1086/176798.
J. F. Gallimore, S. A. Baum, and C. P. O'Dea. *ApJ*, 613(2):794–810, Oct. 2004. doi: 10.1086/423167.
J. F. Gallimore et al. *AJ*, 132(2):546–569, Aug. 2006. doi: 10.1086/504593.
G. Ghisellini et al. *MNRAS*, 438(3):2694–2700, Mar. 2014. doi: 10.1093/mnras/stt2394.
M. Giroletti and F. Panessa. *ApJL*, 706(2):L260–L264, Dec. 2009. doi: 10.1088/0004-637X/706/2/L260.
K. Gültekin et al. *MNRAS*, 516(4):6123–6131, Nov. 2022. doi: 10.1093/mnras/stac2608.
C. L. Hale et al. *MNRAS*, 536(3):2187–2211, Jan. 2025. doi: 10.1093/mnras/stae2528.
M. J. Hardcastle et al. In *Advancing Astrophysics with the SKA – II (AASKAII)*. 2026. arXiv search: Report number AASKAII/Hardcastle01.
C. M. Harrison, D. M. Alexander, J. R. Mullaney, and A. M. Swinbank. *MNRAS*, 441(4):3306–3347, July 2014. doi: 10.1093/mnras/stu515.

C. M. Harrison et al. *Nature Astronomy*, 2:198–205, Feb. 2018. doi: 10.1038/s41550-018-0403-6.
T. M. Heckman and P. N. Best. *ARA&A*, 52:589–660, Aug. 2014. doi: 10.1146/annurev-astro-081913-035722.
T. Hovatta et al. *AJ*, 144(4):105, Oct. 2012. doi: 10.1088/0004-6256/144/4/105.
L. Ighina et al. *A&A*, 647:L11, Mar. 2021. doi: 10.1051/0004-6361/202140362.
Y. Inoue and A. Doi. *ApJ*, 869(2):114, Dec. 2018. doi: 10.3847/1538-4357/aaeb95.
M. Janssen et al. *A&A*, 626:A75, June 2019. doi: 10.1051/0004-6361/201935181.
M. E. Jarvis et al. *MNRAS*, 485(2):2710–2730, May 2019. doi: 10.1093/mnras/stz556.
L. Jiang et al. *ApJ*, 656(2):680–690, Feb. 2007. doi: 10.1086/510831.
P. M. Keller et al. *MNRAS*, 528(4):5692–5702, Mar. 2024. doi: 10.1093/mnras/stae418.
K. I. Kellermann et al. *AJ*, 98:1195, Oct. 1989. doi: 10.1086/115207.
P. Kharb and S. Silpa. *Galaxies*, 11(1):27, Feb. 2023. doi: 10.3390/galaxies11010027.
P. Kharb et al. *ApJ*, 652(1):177–188, Nov. 2006. doi: 10.1086/507945.
J.-S. Kim et al. *A&A*, 690:A129, Oct. 2024. doi: 10.1051/0004-6361/202449663.
R. Kondapally et al. In *Advancing Astrophysics with the SKA – II (AASKAII)*. 2026. arXiv search: Report number AASKAII/Kondapally01.
J. Kormendy and L. C. Ho. *ARA&A*, 51(1):511–653, Aug. 2013. doi: 10.1146/annurev-astro-082708-101811.
R. M. Kratzer and G. T. Richards. *AJ*, 149(2):61, Feb. 2015. doi: 10.1088/0004-6256/149/2/61.
Y. Kudoh et al. In *Advancing Astrophysics with the SKA – II (AASKAII)*. 2026. arXiv search: Report number AASKAII/Kudoh01.
A. Laor and E. Behar. *MNRAS*, 390(2):847–862, Oct. 2008. doi: 10.1111/j.1365-2966.2008.13806.x.
Y. Li et al. VLBI with SKA: Possible arrays and astrometric science, 2024. URL http://arxiv.org/abs/2404.14663.
Y. Liu et al. *ApJ*, 929(1):69, Apr. 2022a. doi: 10.3847/1538-4357/ac5c50.
Y. Liu et al. *ApJL*, 939(1):L5, Nov. 2022b. doi: 10.3847/2041-8213/ac98b2.
Y. Liu et al. *A&A*, 685:A111, May 2024. doi: 10.1051/0004-6361/202449394.
A. P. Lobanov. *A&A*, 330:79–89, Feb. 1998. doi: 10.48550/arXiv.astro-ph/9712132.
P. Madau and M. Dickinson. *ARA&A*, 52:415–486, Aug. 2014. doi: 10.1146/annurev-astro-081811-125615.
M. Mahmud et al. *MNRAS*, 431(1):695–709, May 2013. doi: 10.1093/mnras/stt201.
J. C. McKinney, A. Tchekhovskoy, and R. D. Blandford. *MNRAS*, 423(4):3083–3117, July 2012. doi: 10.1111/j.1365-2966.2012.21074.x.
A. Merloni and S. Heinz. *MNRAS*, 388(3):1011–1030, Aug. 2008. doi: 10.1111/j.1365-2966.2008.13472.x.
A. Merloni, S. Heinz, and T. di Matteo. *MNRAS*, 345(4):1057–1076, Nov. 2003. doi: 10.1046/j.1365-2966.2003.07017.x.
A. Mesinger, B. Greig, and E. Sobacchi. *MNRAS*, 459(3):2342–2353, July 2016. doi: 10.1093/mnras/stw831.
G. Miley and C. De Breuck. *A&ARv*, 15(2):67–144, Feb. 2008. doi: 10.1007/s00159-007-0008-z.
B. Mingo et al. *MNRAS*, 511(3):3250–3271, Apr. 2022. doi: 10.1093/mnras/stac140.
E. Momjian et al. *ApJ*, 861(2):86, July 2018. doi: 10.3847/1538-4357/aac76f.

R. Morganti et al. *A&A*, 580:A1, Aug. 2015. doi: 10.1051/0004-6361/201525860.
D. Mukherjee et al. *MNRAS*, 479(4):5544–5566, Oct. 2018. doi: 10.1093/mnras/sty1776.
I. M. Mutie et al. *MNRAS*, 539(2):808–819, May 2025. doi: 10.1093/mnras/staf524.
N. M. Nagar, H. Falcke, A. S. Wilson, and J. S. Ulvestad. *A&A*, 392:53–82, Sept. 2002. doi: 10.1051/0004-6361:20020874.
N. M. Nagar, H. Falcke, and A. S. Wilson. *A&A*, 435(2):521–543, May 2005. doi: 10.1051/0004-6361:20042277.
R. Narayan and I. Yi. *ApJ*, 452:710, Oct. 1995. doi: 10.1086/176343.
K. Nyland et al. *MNRAS*, 458(2):2221–2268, May 2016. doi: 10.1093/mnras/stw391.
C. P. O'Dea. *PASP*, 110(747):493–532, May 1998. doi: 10.1086/316162.
P. Padovani. *A&ARv*, 24(1):13, Sept. 2016. doi: 10.1007/s00159-016-0098-6.
P. Padovani et al. *A&ARv*, 25(1):2, Aug. 2017a. doi: 10.1007/s00159-017-0102-9.
P. Padovani et al. *A&ARv*, 25(1):2, Aug. 2017b. doi: 10.1007/s00159-017-0102-9.
F. Panessa and M. Giroletti. *MNRAS*, 432(2):1138–1143, June 2013. doi: 10.1093/mnras/stt547.
F. Panessa et al. *Nature Astronomy*, 3:387–396, Apr. 2019. doi: 10.1038/s41550-019-0765-4.
F. Panessa et al. *MNRAS*, 510(1):718–724, Feb. 2022. doi: 10.1093/mnras/stab3426.
K. Perger, S. Frey, K. É. Gabányi, and L. V. Tóth. *Frontiers in Astronomy and Space Sciences*, 4: 9, Aug. 2017. doi: 10.3389/fspas.2017.00009.
P. O. Petrucci et al. *A&A*, 678:L4, Oct. 2023. doi: 10.1051/0004-6361/202347495.
R. M. Plotkin et al. *MNRAS*, 419(1):267–286, Jan. 2012. doi: 10.1111/j.1365-2966.2011.19689.x.
I. Prandoni et al. In *Advancing Astrophysics with the SKA – II (AASKAII)*. 2026. arXiv search: Report number AASKAII/Prandoni01.
J. F. Radcliffe et al. *A&A*, 649:A27, May 2021. doi: 10.1051/0004-6361/202038591.
C. Ricci et al. *ApJL*, 952(2):L28, Aug. 2023. doi: 10.3847/2041-8213/acda27.
I. Ruffa et al. *MNRAS*, 522(4):6170–6195, July 2023. doi: 10.1093/mnras/stad1119.
P. Saikia, E. Körding, and S. Dibi. *MNRAS*, 477(2):2119–2127, June 2018. doi: 10.1093/mnras/sty754.
M. T. Sargent et al. *ApJSS*, 186(2):341–377, Feb. 2010. doi: 10.1088/0067-0049/186/2/341.
T. Sbarrato et al. *MNRAS*, 426(1):L91–L95, Oct. 2012. doi: 10.1111/j.1745-3933.2012.01332.x.
B. Sebastian et al. *MNRAS*, 499(1):334–354, Nov. 2020. doi: 10.1093/mnras/staa2473.
E. Shablovinskaya et al. *A&A*, 690:A232, Oct. 2024. doi: 10.1051/0004-6361/202450133.
M. Sikora, Ł. Stawarz, and J.-P. Lasota. *ApJ*, 658(2):815–828, Apr. 2007. doi: 10.1086/511972.
S. Silpa et al. *MNRAS*, 507(1):991–1001, Oct. 2021a. doi: 10.1093/mnras/stab1870.
S. Silpa et al. *MNRAS*, 507(2):2550–2561, Oct. 2021b. doi: 10.1093/mnras/stab2110.
S. Silpa et al. *MNRAS*, 513(3):4208–4223, July 2022. doi: 10.1093/mnras/stac1044.
C. Spingola et al. *A&A*, 643:L12, Nov. 2020. doi: 10.1051/0004-6361/202039458.
C. Spingola et al. In *Advancing Astrophysics with the SKA – II (AASKAII)*. 2026. arXiv search: Report number AASKAII/Spingola01.
A. Tchekhovskoy, R. Narayan, and J. C. McKinney. *MNRAS*, 418(1):L79–L83, Nov. 2011. doi: 10.1111/j.1745-3933.2011.01147.x.
J. S. Ulvestad and L. C. Ho. *ApJ*, 558(2):561–577, Sept. 2001. doi: 10.1086/322307.
J. S. Ulvestad and A. S. Wilson. *ApJ*, 285:439–452, Oct. 1984. doi: 10.1086/162520.
J. S. Ulvestad, R. R. J. Antonucci, and R. W. Goodrich. *AJ*, 109:81, Jan. 1995. doi: 10.1086/117258.

M. Volonteri, M. Sikora, and J.-P. Lasota. *ApJ*, 667(2):704–713, Oct. 2007. doi: 10.1086/521186.
A. Wang et al. *MNRAS*, 504(3):3823–3830, July 2021. doi: 10.1093/mnras/stab587.
A. Wang et al. *MNRAS*, 518(1):39–53, Jan. 2023a. doi: 10.1093/mnras/stac3091.
A. Wang et al. *MNRAS*, 523(1):L30–L34, July 2023b. doi: 10.1093/mnrasl/slad051.
A. Wang et al. *MNRAS*, 525(4):6064–6083, Nov. 2023c. doi: 10.1093/mnras/stad2651.
A. Wang et al. *ApJL*, 987(2):L26, July 2025. doi: 10.3847/2041-8213/ade14a.
Y. Wang et al. *A&A*, 689:A327, Sept. 2024. doi: 10.1051/0004-6361/202449732.